THEMIS multi-spacecraft observations of a reconnecting magnetosheath current sheet with symmetric boundary conditions and a large guide field

M. Øieroset[1], T. D. Phan[1], M. A. Shay[2], C. C. Haggerty[2], M. Fujimoto[3], V. Angelopoulos[4], J. P. Eastwood[5], and F. S. Mozer[1]

[1]Space Sciences Laboratory, University of California, Berkeley, California, USA

[2]Department of Physics and Astronomy, University of Delaware, Newark, Delaware, USA

[3]ISAS/JAXA, Sagamihara, Japan

[4] Institute of Geophysics and Planetary Physics, University of California, Los Angeles, California, USA

[5]The Blackett Laboratory, Imperial College London, London, UK

SHORT TITLE: GUIDE FIELD MAGNETOSHEATH RECONNECTION

Key points

- First multi-spacecraft observations of oppositely directed reconnection exhausts in the magnetosheath
- First observations of two colliding reconnection jets wrapped around each other
- Asymmetric plasma and field profiles in the exhaust due to large guide field

Abstract We report three spacecraft observations of a reconnecting magnetosheath current sheet with a guide field of unity, with THD and THE/THA observing oppositely directed reconnection exhausts, indicating the presence of an X-line between the spacecraft. The near constant convective speed of the magnetosheath current sheet allowed the direct translation of the observed time series into spatial profiles. THD observed asymmetries in the plasma density and temperature profiles across the exhaust, characteristics of symmetric reconnection with a guide field. The exhausts at THE and THA, on the other hand, were not the expected mirror image of the THD exhaust in terms of the plasma and field profiles. They consisted of a main outflow at the center of the current sheet, flanked by oppositely directed flows at the two edges of the current sheet, suggesting the presence of a second X-line, whose outflow wraps around the outflow from the first X-line.

Index Terms

7835 Magnetic reconnection (2723)

2728 Magnetosheath

7845 Particle acceleration

1. Introduction

Magnetic reconnection is a universal energy conversion process that converts magnetic energy into particle energy. In-situ observations in the Earth's magnetosphere have provided unambiguous evidence for the occurrence of reconnection by detecting the reconnection exhaust as well as the diffusion region [e.g. Paschmann et al. 1979, 2013; Burch et al., 2016]. However, many key questions concerning the fundamental spatial and temporal nature of reconnection have not been answered by observations in the magnetosphere, where both the boundary conditions and the motion of current sheets can be highly varying.

Current sheets in the solar wind [e.g., Gosling et al., 2005, 2007; Phan et al., 2006, 2009; Eriksson et al., 2015; Mistry et al., 2016] and in the magnetosheath [e.g., Phan et al., 2007a,b; Retino et al., 2007] provide ideal environments for reconnection studies. These current sheets convect at nearly constant speeds past a spacecraft, conditions that are rare in the magnetosphere. The constant speed allows the direct translation of the observed time series into spatial profiles. Furthermore, the magnetosheath contains current sheets with symmetric boundary conditions and large guide fields. Such current sheets are rare in the magnetosphere, where reconnection is typically highly asymmetric at the magnetopause, while reconnection in the magnetotail is normally symmetric with small (<< 50%) guide fields.

In this paper we present a magnetosheath event where three THEMIS spacecraft observed diverging reconnection jets on opposite sides of an X-line in a nearly symmetric current sheet with a guide field near unity. The two sides of the X-line displayed significant differences, and we attribute the differences to the presence of a magnetic island/flux rope on one side of the X-line, and a regular (open-ended) exhaust on the other side.

The paper is organized as follows. In section 2 we describe the spacecraft instrumentation. In sections 3-6 we present detailed observations of the exhaust profile on each side of the X-line. In section 7 we qualitatively compare the observations with a 2.5-D particle-in-cell (PIC) simulation. The results are summarized and discussed in section 8.

2. Instrumentation

We use 3 s resolution ion and electron data from the electrostatic analyzer (ESA) [McFadden et al., 2008] and 128 samples/s data from the fluxgate magnetometer (FGM) [Auster et al., 2008] and the electric field instrument (EFI) [Bonnell et al., 2008] onboard the THEMIS spacecraft [Angelopoulos, 2008]. The THEMIS high resolution burst mode [Phan et al., 2016] was triggered onboard all three spacecraft by the sharp variations in the GSE-z component of the magnetic field across the current sheet. The data are presented in the geocentric solar ecliptic (GSE) coordinate system and in the LMN boundary normal coordinate system of the magnetosheath current sheet, with positive N directed along the current sheet normal and sunward, M along the X-line, and L along the reconnecting field direction.

3. Overview of Three-Spacecraft Observations

On October 31, 2010, between 16:49 UT and 16:52 UT, THEMIS-A (THA), THEMIS-D (THD), and THEMIS-E (THE) were in the magnetosheath upstream of the Earth's magnetopause (Fig.1a).

Figures 1c-h show the THD, THE, and THA magnetic field and ion velocity observations in GSE coordinates. All three spacecraft observed a rotation in B_Z and B_Y accompanied by plasma jetting (relative to the magnetosheath flows outside the current sheet), indicating the passage of a reconnecting current sheet.

We determined the current sheet normal (LMN) coordinate system by the minimum variance analysis of the magnetic field (MVAB) [Sonnerup and Cahill, 1967] across the current sheet. The resulting LMN directions determined separately for the three spacecraft differ by less than 7° for any component. To describe the overall geometry of the current sheet and the relative locations of the spacecraft we use a common LMN coordinate system, which we choose to be that of THE. However, for the determination of the reconnection inflow velocity and the reconnection rate at each spacecraft, which requires more accurate knowledge of the current sheet normal, we use the normal determined at each spacecraft.

Fig.1b displays the spacecraft positions at 16:50:00 UT projected onto the L-N plane. The current sheet convected anti-sunward, in the negative N direction. Relative to THD, THE was located 803 km (15 d_i) in the -N direction and 2361 km (44 d_i) in the -L direction, whereas THA was located 682 km (13 d_i) in the -N direction and 2960 km (55 d_i) in the –L direction, where d_i =54 km based on the observed magnetosheath ion density of 18 cm^{-3}. The maximum spacecraft separation along M was 2631 km (49 d_i).

Fig.1i-n show the observations in LMN coordinates. The guide field B_M (measured outside the current sheet) was ~1.2 times the reconnecting magnetic field B_L. During the current sheet crossing THD observed a positive V_L jet, while both THA and THE observed a negative V_L jet at the current sheet midplane (B_L=0). The relative positions of the spacecraft and the oppositely directed jets seen at THD and THE/THA imply that the jets were diverging, indicating the presence of an X-line between THD and THE/THA. This scenario is illustrated in Fig.2a. Fig.2 (simulation) will be discussed in detail in section 7.

The V_L jet speed at midplane (relative to the average external magnetosheath flow of V_L~35 km/s) was different at the three spacecraft, with peak jet speed ~100 km/s at THD, ~ 90 km/s at THE, and 70 km/s at THA.

The V_L jet structures were also different on the two sides of the X-line: While the THD jet was unidirectional throughout the exhaust, the dominant, negative V_L jet at the midplane observed by THE and THA (Fig.2l,n) was flanked by two weaker, positive V_L flows at the edges of the exhaust. This tripolar jet profile suggests that a second X-line could be present, giving rise to positive V_L flows (relative to the asymptotic magnetosheath V_L) at the exhaust edges at THE/THA. The slower jet speed at THE and THA at the midplane would also be consistent with the presence of a second X-line providing an obstacle to the flow.

The current sheet midplane (B_L=0) was encountered first by THD at 16:49:56 UT, followed by THA at 16:50:24 UT, and by THE at 16:50:48 UT. Assuming a planar structure, the current sheet propagation speed in the normal direction based on when B_L=0 at each spacecraft was 15.4 km/s from THD to THE, 24.4 km/s from THD to THA, and 5.0 km/s from THA to THE. We found similar inconsistencies in the propagation speeds using other markers such as the time of the exhaust leading edge and the sudden changes in B_M or density. Thus timing the structures does not work in this case, likely because the structures are too different at each spacecraft. As will be discussed below (section 6) the results are more consistent if one infers the current sheet propagation speed from the average V_N measured on the two sides of the current sheet.

4. THEMIS-D observations: Open-ended exhaust?

4.1. Overview

Fig.3 shows THD observations in and around the current sheet. Because the estimation of the reconnection rate locally requires accurate determination of the boundary normal, we determined the LMN coordinates in Fig.3 using MVAB of the local THD crossing (16:49:42 – 16:50:24 UT).

The leading edge of the exhaust (solid vertical line L) is marked by sudden changes in the magnetic field (Fig.3a), density (Fig.3d,e), temperatures (Fig.3f,g), and velocity (Fig.3c). The trailing edge is less well defined since the locations where the plasma and fields reached their asymptotic magnetosheath values were not the same. However, 16:50:01 UT (the vertical solid line marked T1) is a likely location of the trailing edge. This is where the ion V_L jetting (Fig.4c) and strong electric field (Fig.3l) stopped, as well as where the ion and electron temperatures (Fig.3f,g), ion and electron spectrograms (Fig.3h-k), and electron distributions (not shown) are essentially the same as in the magnetosheath proper to the right. The only feature which seems inconsistent with this location being the exhaust edge is the value of B_L not being the same as in the asymptotic magnetosheath. The field rotation across the current sheet is 65° at this location versus 80° for the full rotation to the asymptotic state at 16:50:25 UT (vertical dashed line T2). The precise location of the trailing edge does not affect our discussion below of the asymmetries of the plasma and field profiles in the exhaust (Section 4.2). However, it does affect the estimate of the distance to the X-line.

The plasma density (Fig.3d,e), temperatures (Fig.3f,g) and the B_L strength (Fig.3a) in the two inflow regions were similar, except for the ion temperature which was about 40% higher on the trailing edge. Thus this is essentially symmetric reconnection (with a guide field of near unity).

There was a velocity shear of 21 km/s across the current sheet in the L direction, which is 14% of the inflow Alfven speed (154 km/s) based on B_L (assuming that all ions were protons). The velocity shear in the M direction was 29 km/s.

The THD reconnection jet reached a maximum speed of ΔV_L~100 km/s (relative to the average external magnetosheath V_L of -35 km/s) at 16:49:53 UT. This is 65% of the inflow Alfven speed based on B_L.

4.2. Plasma and field profiles

The plasma and field structures in the exhaust displayed large asymmetries. Left of midplane (marked M in Figure 3) the plasma density was enhanced, and to the right it was depressed (Fig.3d,e). Asymmetries were also seen in the perpendicular and parallel ion temperatures, with $T_{i||}$ enhanced on the side of the exhaust where the density was depressed and a local peak in $T_{i\perp}$ on the high-density side (Fig.3f). Furthermore, the parallel electron temperature was strongly enhanced on the high density side while $T_{e\perp}$ displayed slight cooling throughout the exhaust (Fig.3g). The electron temperature effects can also be seen in the enhancements of thermal (~40-200 eV) electron fluxes at 0° and 180° pitch angles inside the exhaust, accompanied by a decrease in thermal electron flux at 90° (Fig.3i-k).

The out-of-plane magnetic field B_M displayed a bipolar perturbation relative to the guide field and is shunted away from the mid-plane (Fig.3b). The normal component of the electric field E_N was predominantly negative at the center of the current sheet, and positive at the exhaust edges. These asymmetries are likely associated with guide field effects [Eastwood et al., 2010; Mistry et al., 2016; Oieroset et al., 2016].

5. THEMIS-A and THEMIS-E observations: Evidence for a second X-line?

With THE/THA being on the opposite side of the X-line from THD, one would expect that the guide field associated plasma and field asymmetries across the exhaust detected at THE/THA would be opposite to those of THD. However, the profiles at THE and THA are more complex.

One would expect that on this side of the X-line, E_N should be predominantly positive, the parallel electron heating, ion perpendicular heating, and density compression should be shifted to the right of the midplane, while parallel ion heating would be shifted to the left. Such behaviors were indeed seen at THE (Fig.4a-l) and THA (Fig.4m-x). However, there were additional features in the density and temperature profiles that are not expected: There were enhancements of $T_{e||}$, $T_{i\perp}$ and density to the left of the midplane at both THE and THA. Furthermore, the negative V_L jet did not span the entire current sheet. A negative V_L jet was seen near midplane, flanked by slower positive V_L flows close to the two edges of the current sheet. At THE the negative V_L jet occupied a bigger portion of the current sheet than at THA, which was located further from the main X-line. At THA, the flanking positive V_L jets were broader.

The observed flow pattern at THE and THA suggests the presence of a second X-line beyond THA (in the negative L direction), such that THE and THA were located between two active X-lines. In this scenario, the negative V_L near the midplane originated from the first X-line, while the positive V_L near the edges of the current sheet come from the second X-line. In addition to explaining the unusual flow pattern, the second X-line scenario could also account for the unexpected parallel electron heating and density compression seen on the left side of midplane.

The two X-line scenario may also be consistent with the observed out-of-plane B_M profile. B_M observed by both THE and THA displayed negative to positive variations near the left edge of the exhaust (Figures 4b and 4n), similar to the B_M observed by THD on the opposite side of the X-line (Fig.3b). This is inconsistent with the single X-line picture where the polarities of the Hall magnetic fields should flip from one side of the X-line to the other. In the two X-line scenario, the observed B_M dip near the leading edge seen at THE and THA would be associated with the second X-line.

In summary, the exhaust profiles observed by THE and THA did not simply display the opposite asymmetries as those observed by THD. Instead, the THE and THA exhaust profiles may be the results of the combined effects from two converging reconnection exhausts forming a magnetic flux rope.

6. Current sheet speed, thickness, reconnection rate and estimated distance to X-line

In Section 3 we pointed out that the current sheet propagation speed was not well determined by the timing analysis using pairs of spacecraft. Here we estimate the normal motion of the current sheet at each spacecraft individually based on the average of V_N on the two sides of the current sheet. The average V_N was ~14.7 km/s for THD, ~16.8 km/s for THE and ~17.7 km/s for THA, where the V_N values on each side of the current sheet were calculated using a 60 s interval starting 15 s away from each exhaust edge (to avoid structures around the exhaust boundaries).

Using these V_N speeds, the exhaust widths at THD, THE and THA were estimated to be 220 km (4.1 d_i), 689 km (13 d_i) and 956 km (18 d_i) based on the exhaust crossing times of 15s, 41s, and 54s, respectively.

At all three spacecraft, there was a negative shift in V_N across the current sheet. In the frame of the convecting current sheet, the negative ΔV_N is consistent with reconnection inflows from the two sides of the current sheet. The measured inflow speed ($\Delta V_N/2$) were ~6.6 km/s at THD, ~8.0 km/s at THE, and ~8.2 km/s at THA. The corresponding dimensionless reconnection rate, $V_N/V_{AL,inflow}$, was 0.043 at THD, 0.052 at THE and 0.053 at THA based on the inflow B_L of 30 nT and a density of 18 cm^{-3}.

The good agreements between the reconnection rates determined independently at the three spacecraft may suggest that the measured rate of ~0.05 is reliable. However, with the reconnection rate of 0.043 and an exhaust thickness of 4.1 d_i, the estimated distance from THD to the X-line is 48 d_i, which places the X-line past THE, which was located 44 d_i from THD along the –L direction. This is inconsistent with the location of an X-line between THE and THD based on the detection of diverging jets. Similarly, at THE and THA, the 13d_i and 18 d_i thick current sheets together with a reconnection rate of 0.05 place the estimated location of the X-line tens of d_i beyond THD (in the +L direction), again inconsistent with the observed positive V_L detected at THD.

An alternative approach to calculate the reconnection rate is to use the multipoint measurements to reconstruct the opening angle of the exhaust. If it is assumed that the reconnection exhausts expand linearly on both sides of the X-line, the reconnection rate has to be ~0.2 to be consistent with the distances between the three spacecraft and the X-line being located between THE and THD. However, the assumption of a linearly expanding (constant angle) exhaust may not be consistent with the presence of a magnetic island/flux rope at the THE/THA location as the plasma and field profiles suggest (section 5).

If one were to use the canonical reconnection rate of 0.1 instead, the estimated X-line location would be 20.5 d_i from THD, between THD and THE. This would be consistent with the diverging jet observations. However, using the THE or THA data with an assumed reconnection rate of 0.1, and assuming linear expansion, still places the X line beyond THD. However, if THE and THA were in a flux rope/island flanked by two X-lines, the bulging of the field lines associated with the flux rope would lead to substantial widening of the exhaust and could account for the thick current sheet at THE and THA, as we discuss below with the help of a simulation.

The multi-spacecraft analysis above illustrates that reconnection rates must be calculated with care. Local measures were shown to be inconsistent with the large-scale picture, and simple geometrical calculations can also be wrong if the exhaust is distorted by the presence of an island. Thus the determination of the reconnection rate experimentally continues to be a challenge.

7. Comparison with simulation

We now compare the THEMIS observations with a 2-D particle-in-cell simulation involving symmetric reconnection with a guide field of unity (Fig.2). The simulation parameters are similar but not identical to the observations, especially the lack of observed inflow ion temperature anisotropy in the simulation. Figure 2a shows V_{iL} in the L-N plane. The plot is periodic in L, thus the island is surrounded by two X-lines. The comparison is intended to be qualitative and serves mainly to illustrate the presence of colliding jets (from two X-lines) that wrap around each other and the bulging of the exhaust due to the presence of an island.

First we examine the plasma and field profiles to the right of the X-line at a location (L=18.9 d_i) far from the magnetic island and its associated jet pileup region. At this location the exhaust profile displays magnetic field B_M, density and temperature asymmetries that resemble those at THD, namely the enhancements of density (Fig.2l), ion perpendicular heating (Fig.2m), electron parallel heating (Fig.2n) on the left side of the exhaust, and ion parallel heating (Fig.2m) and density depression (Fig.2l) shifted to the right side.

On the other side of the X-line the two converging jets (from the two X-lines) wrap around each other (Fig.2a). The profiles near the center of the island (Fig.2b-h) show some features that are similar to those observed at THE/THA, namely the presence of tripolar V_{iL}, with a negative V_{iL} jet near midplane flanked by positive V_{iL} flows near the exhaust edges (Fig.2d), and the presence of two enhancements in the electron parallel temperature and a dip near the midplane (Fig.2g). The B_M, density and ion temperature profiles, on the other hand, are less similar to the observations (Fig.2c,e,f). The bulging of the exhaust due to the island formation leads to a non-linear expansion of the exhaust, which could be consistent with THE/THA detecting a thicker than expected exhaust. Some disagreements between the observations and the simulation are not unexpected, especially since the island in the simulation is continuously evolving. Furthermore, the “two X-lines” in the simulation are the same X-line (due to periodic boundary conditions), thus they were formed simultaneously. In reality, the two X-lines could have formed at different times (Fig.2p), in which case outflows from the left X-line could wrap around the outflows from the right X-line, further contributing to a tripolar V_{iL} profile as observed by THA and THE.

8. Summary and discussion

We have presented an event where three THEMIS spacecraft crossed a reconnecting magnetosheath current sheet with near-symmetric inflow conditions and a guide field of 1.2, conditions that are rare in the magnetosphere. The three THEMIS spacecraft recorded detailed exhaust profiles, with THD observing a positive V_L jet and THE and THA observing a main jet in the negative L direction. The oppositely directed V_L jets observed by THD and THE/THA indicate that THD and THE/THA were located on opposite sides of an X-line.

The two diverging exhausts displayed significant differences. THD observed a unidirectional jet, resembling an open-ended exhaust, while THE and THA observed return flows along the exhaust edges, suggesting that THE and THA crossed a magnetic island/flux rope between two active X-lines.

The open-ended exhaust was characterized by large asymmetries in plasma profiles. Ion perpendicular heating, electron parallel heating, and density compression were observed on one side of the exhaust, while ion parallel heating and density depression were shifted to the other side. The key to these asymmetries is the guide field. The large guide field and the outflow lead to a normal electric field that span across the exhaust. Entering ions move in the direction of the electric field in cusp-like orbits [Drake et al., 2009 Drake et al., 2014; Pritchett and Coroniti, 2004], resulting in the perpendicular temperature and density being larger on the side where E_N points toward the inflow. Furthermore, in guide field reconnection, electron are accelerated toward the X-line along two of the four separatrices and ejected out along the opposite sides of the exhaust, leading to quadrupolar density structures in the exhausts [Pritchett and Coroniti, 2004] and enhanced electron temperature on the high density side of the exhaust where accelerated and inflowing electrons are mixed [Drake et al., 2005]. Such asymmetries were recently observed in a thin reconnection layer at the center of a magnetopause flux rope by MMS

[Øieroset et al., 2016]. The quadrupolar density behavior was also seen in a laboratory experiment [Fox et al., 2017].

The asymmetries in the plasma and field profiles were expected to reverse on the opposite side of an X-line, but the density, temperature, and B_M profiles at THE and THA were more complex, and largely consistent with the combined effects of two X-lines flanking THE/THA, forming a magnetic island/flux rope.

Acknowledgements

This research was supported in part by NSF grant AGS-1103303, NASA grants NNX13AD72G, NNX08AO83G, NNX15AW58G, and STFC(UK) grant ST/N000692/1. Simulations performed at the National Center for Atmospheric Research. Data source: THEMIS Data Center at themis.ssl.berkeley.edu.

References

Angelopoulos, V. (2008), The THEMIS mission, Space Sci. Rev. 141, 4, doi:10.1007/s11214-008-9336-1.

Auster, H. U., K. H. Glassmeier, W. Magnes, O. Aydogar, W. Baumjohann, D. Constantinescu, D. Fischer, K. H. Fornacon, E. Georgescu, P. Harvey, O. Hillenmaier, R. Kroth, M. Ludlam, Y. Narita, R. Nakamura, K. Okrafka, F. Plaschke, I. Richter, H. Schwarzl, B. Stoll, A. Valavanoglou, and M. Wiedemann (2008), The THEMIS Fluxgate Magnetometer, Space Sci. Rev. 235, 303, doi:10.1007/s11214-008-9365-9.

Bonnell, J. W., F. S. Mozer, G. T. Delory, A. J. Hull, R. E. Ergun, C. M. Cully, V. Angelopoulos, and P. R. Harvey (2008), The Electric Field Instrument (EFI) for THEMIS, Space Sci. Rev. 141, 303, doi:10.1007/s11214-008-9469-2.

Burch, J. L., et al. (2016), Electron-scale measurements of magnetic reconnection in space, Science, 352(6290), aaf2939, doi:10.1126/science.aaf2939.

Drake, J. F., M. A. Shay, W. Thongthai, and M. Swisdak (2005), Production of energetic electrons during magnetic reconnection, Phys. Rev. Lett., 94, 095001, doi:10.1103/PhysRevLett.94.095001.

Drake, J. F., P. A. Cassak, M. A. Shay, M. Swisdak, and E. Quataert (2009), A magnetic reconnection mechanism for ion acceleration and abundance enhancements in impulsive flares, *The Astrophysical Journal*, 700:L16–L20, doi:10.1088/0004-637X/700/1/L16.

Drake, J. F., and M. Swisdak (2014), The onset of ion heating during magnetic reconnection with a strong guide field, *Phys. Plasmas*, 21, 072903, doi: 10.1063/1.4889671.

Eastwood, J. P., M. A. Shay, T. D. Phan, and M. Øieroset (2010), Asymmetry of the Ion Diffusion Region Hall Electric and Magnetic Fields during Guide Field Reconnection: Observations and Comparison with Simulations, Phys. Rev. Lett. 104, 205001.

Eriksson, S. G. Lapenta, D. L. Newman, T. D. Phan, J. T. Gosling, B. Lavraud, Yu. V. Khotyaintsev, C. M. Carr, S. Markidis, and M. V. Goldman (2015), On multiple reconnection X-lines and tripolar perturbations of strong guide magnetic fields, Ap. J., 805:43, doi: 10.1088/0004-637X/805/1/43.

Fox, W., F. Sciortino, A. v. Stechow, J. Jara-Almonte, J. Yoo, H. Ji, and M. Yamada (2017), Experimental Verification of the Role of Electron Pressure in Fast Magnetic Reconnection with a Guide Field, Phys. Rev. Lett. 118, 125002.

Gosling, J. T., R. M. Skoug, D. J. McComas, and C. W. Smith (2005), Direct evidence for magnetic reconnection in the solar wind near 1 AU, J. Geophys. Res., 110, A01107, doi:10.1029/2004JA010809.

Gosling, J. T., S. Eriksson, T. D. Phan, D. E. Larson, R. M. Skoug, and D. J. McComas (2007), Direct evidence for prolonged magnetic reconnection at a continuous x-line within the heliospheric current sheet, Geophys. Res. Lett., 34, L06102, doi:10.1029/2006GL029033.

McFadden, J. P., C.W. Carlson, D. Larson, M Ludlam, R. Abiad, B. Elliott, P. Turin, M. Marckwordt, M., and V. Angelopoulos (2008), The THEMIS ESA Plasma Instrument and In-flight Calibration, Space Sci. Rev. 141, 277, doi:10.1007/s11214-008-9440-2.

Mistry, R., J. P. Eastwood, C. C. Haggerty, M. A. Shay, T. D. Phan, H. Hietala, and P. A. Cassak (2016), Observations of Hall Reconnection Physics Far Downstream of the X Line, Phys. Rev. Lett. 117, 185102, doi:https://doi.org/10.1103/PhysRevLett.117.185102.

Mistry, R., J. P. Eastwood, T. D. Phan, and H. Hietala, Statistical properties of solar wind reconnection exhausts, J. Geophys. Res. Space Physics, in press, 2017, doi:10.1002/2017JA024032.

Øieroset, M. et al. (2016), MMS observations of large guide field symmetric reconnection between colliding reconnection jets at the center of a magnetic flux rope at the magnetopause, Geophys. Res. Lett., 42, doi:10.1002/2016GL069166.

Paschmann, G., B. U. Ö. Sonnerup, I. Papamastorakis, N. Sckopke, G. Haerendel, S. J. Bame, J. R. Asbridge, J. T. Gosling, C. T. Russell and R. C. Elphic (1979), Plasma acceleration at the Earth's magnetopause: evidence for reconnection, Nature, 282, 243 - 246 (15 November 1979), doi:10.1038/282243a0.

Paschmann, G., Øieroset, M. & Phan, T. (2013), In-situ observations of reconnection in space, Space Sci. Rev. 178: 385. doi:10.1007/s11214-012-9957-2.

Phan, T. D. et al (2006), A magnetic reconnection X-line extending more than 390 Earth radii in the solar wind, Nature 439, 175-178 (12 January 2006), doi:10.1038/nature04393

Phan, T. D., J. F. Drake, M. A. Shay, F. S. Mozer, and J. P. Eastwood (2007a), Evidence for an Elongated (>60 Ion Skin Depths) Electron Diffusion Region during Fast Magnetic Reconnection, Phys. Rev. Lett. 99, 255002.

Phan, T. D., G. Paschmann, C. Twitty, F. S. Mozer, J. T. Gosling, J. P. Eastwood, M. Øieroset, H. Rème, and E. A. Lucek (2007b), Evidence for magnetic reconnection initiated in the magnetosheath, Geophys. Res. Lett., 34, L14104, doi:10.1029/2007GL030343.

Phan, T. D., J. T. Gosling, and M. S. Davis (2009), Prevalence of extended reconnection X-lines in the solar wind at 1 AU, Geophys. Res. Lett., 36, L09108, doi:10.1029/2009GL037713.

Phan, T.D., M. A. Shay, J. P. Eastwood, V. Angelopoulos, M. Øieroset, M. Oka, and M. Fujimoto (2016), Establishing the Context for Reconnection Diffusion Region Encounters and Strategies for the Capture and Transmission of Diffusion Region Burst Data by MMS, Space Sci. Rev. 199: 631. doi:10.1007/s11214-015-0150-2.

Pritchett, P. L., and F. V. Coroniti (2004), Three-dimensional collisionless magnetic reconnection in the presence of a guide field, J. Geophys. Res., 109, A01220, doi:10.1029/2003JA009999.

Retino, A., D. Sundkvist, A. Vaivads, F. Mozer, M. André and C. J. Owen (2007), In situ evidence of magnetic reconnection in turbulent plasma, Nature Physics 3, 235 - 238, doi:10.1038/nphys574.

Sonnerup, B. U. Ö., and L. J. Cahill Jr. (1967), Magnetopause structure and attitude from Explorer 12 observations, *J. Geophys. Res.*, 72, 171.

Figure 1. (a) THEMIS spacecraft positions at 17:50 UT on 2010-10-31, projected onto the GSE x-y plane. The dashed line indicates the model magnetopause. THD was located at $(x,y,z)_{GSE}$=(11.14, -1.22, 2.65)R_E, THA at (11.07, -1.77, 2.35)R_E, and THE at (11.05, -1.61, 2.39)R_E. (b) Spacecraft positions projected onto the L-N plane in a common current sheet normal coordinate system (LMN) determined by MVAB at THE (16:50:21-16:51:12 UT). L=GSE[-0.146,0.348,0.926], M=GSE[0.130,0.935,-0.330], and N=GSE[0.981,-0.072,0.182]. (c)-(h) THD, THE, and THA magnetic field and ion velocity in GSE, (i)-(n) THD, THE, and THA magnetic field and ion velocity in LMN.

Figure 2. Results from a 2D PIC simulation. Details of the simulation are in the Supplementary Material section. (a) 2D plot of V_{iL} in the L-N plane. Red and blue denote flows in the positive and negative L direction, respectively. (b)-(h) plasma and field parameters along a cut at L=-41.7 d_i, near the center of the island, showing tripolar V_L flows and double enhancements of $T_{e||}$ similar to the THE/THA observations. (i)-(o) Plasma and field parameters along a cut at L= 18.9 d_i, showing "open exhaust" profiles that are similar to THD observations. The direction of the virtual spacecraft trajectories from -N to +N mimics the +N spacecraft motion through the current sheet (as depicted also in Fig.1b). (p) Cartoon showing how reconnection jets can wrap around each other when two X-lines form at different times.

Figure 3. THD observations in LMN coordinates determined by MVAB at THD. (a) magnetic field, (b) out of plane magnetic field, (c) ion velocity, (d) density derived from the spacecraft potential, (e) ion density, (f) ion temperatures, (g) electron temperatures, (h) ion energy spectrogram, (i)-(k) electron energy spectrogram at 180°, 90°, and 0° pitch angles, and (l)

electric field. The solid vertical lines mark the current sheet edges, where L marks the leading edge and T1 and T2 marks two candidates for the trailing edge. The dashed vertical line denotes B_L=0 time.

Figure 4. THE (a-l) and THA (m-x) observations in LMN, using the same formats as in Fig.3. The solid vertical lines mark the edges of the current sheet and the dashed vertical line denotes B_L=0 time. LMN coordinates determined by MVAB of the local THE and THA crossings (at 16:50:21–16:51:12UT and 16:49:58–16:51:05UT, respectively).

Figure 1.

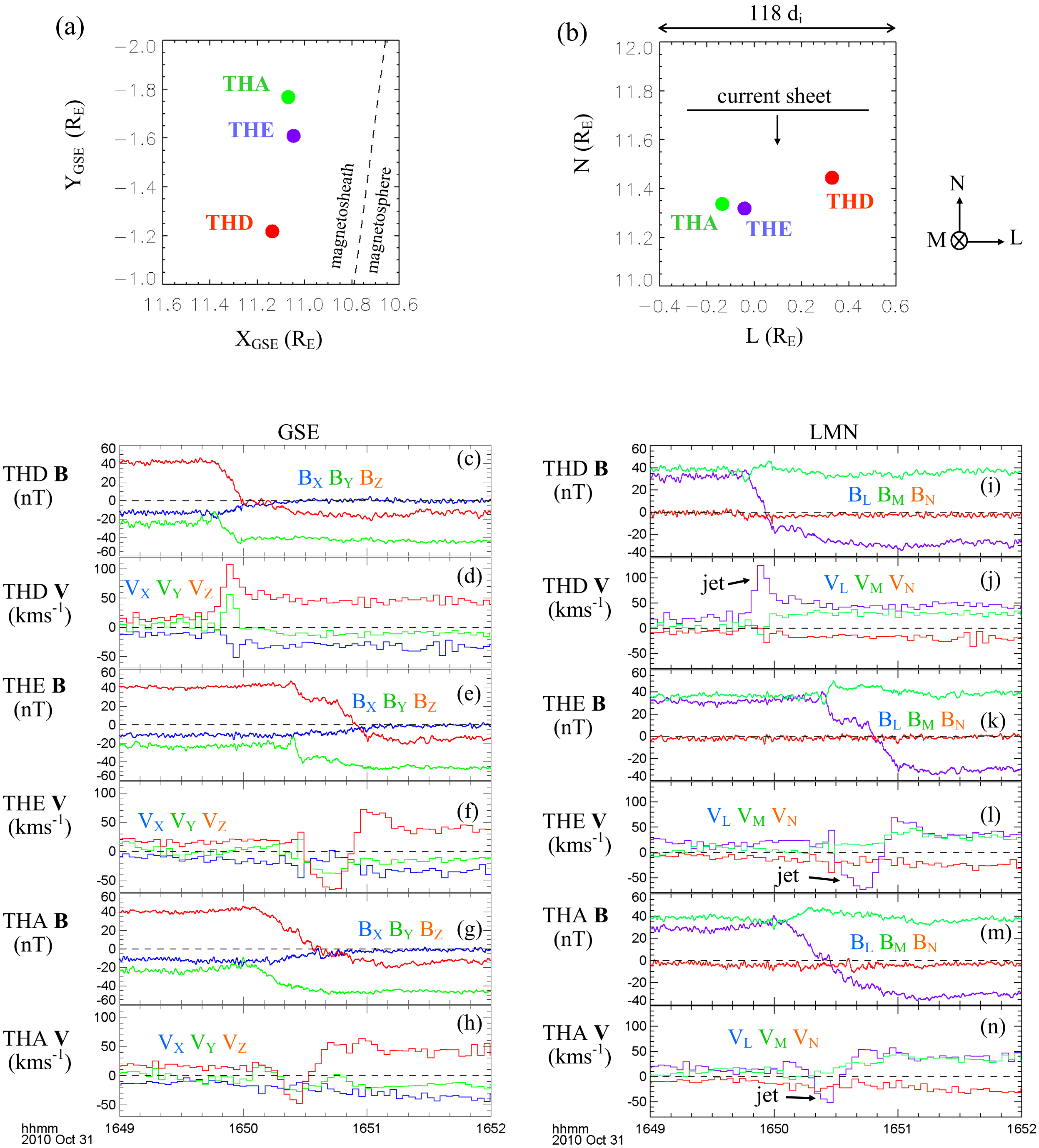

(a)
THA
THE
THD
magnetosheath
magnetosphere
Y_{GSE} (R_E)
X_{GSE} (R_E)
(b)
118 d_i
current sheet
THA
THE
THD
N (R_E)
L (R_E)
N
M
L
GSE
LMN
THD **B** (nT)
THD **V** (kms^{-1})
THE **B** (nT)
THE **V** (kms^{-1})
THA **B** (nT)
THA **V** (kms^{-1})
B_X B_Y B_Z
V_X V_Y V_Z
B_L B_M B_N
V_L V_M V_N
jet
hhmm
2010 Oct 31
1649
1650
1651
1652

Figure 2.

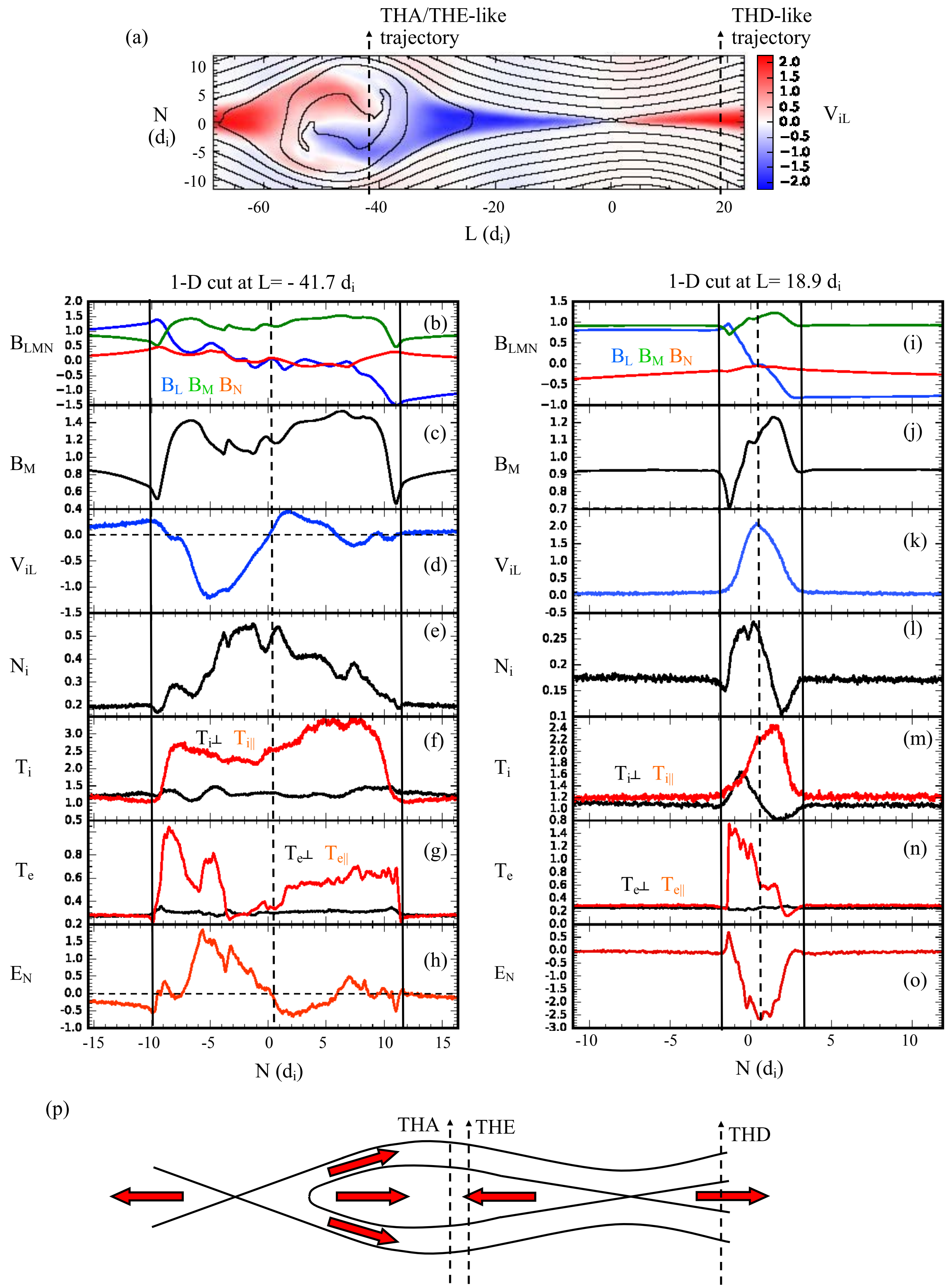

(a)
THA/THE-like trajectory
THD-like trajectory
N (d$_i$)
L (d$_i$)
V_{iL}
1-D cut at L= - 41.7 d$_i$
1-D cut at L= 18.9 d$_i$
B_{LMN}
B_L B_M B_N
B_M
V_{iL}
N_i
T_i
$T_{i\perp}$ $T_{i||}$
T_e
$T_{e\perp}$ $T_{e||}$
E_N
(b) (c) (d) (e) (f) (g) (h)
(i) (j) (k) (l) (m) (n) (o)
N (d$_i$)
(p)
THA
THE
THD

Figure 3.

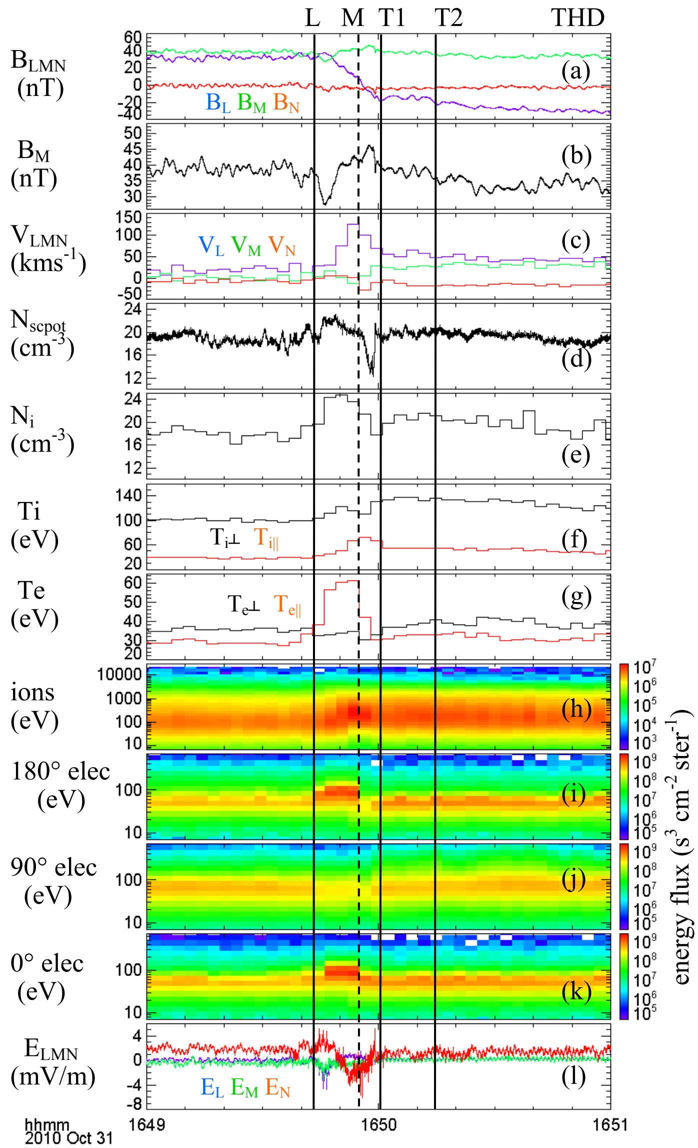

L M T1 T2 THD
B_LMN (nT)
B_L B_M B_N
(a)
B_M (nT)
(b)
V_LMN (kms^-1)
V_L V_M V_N
(c)
N_scpot (cm^-3)
(d)
N_i (cm^-3)
(e)
Ti (eV)
Ti⊥ Ti||
(f)
Te (eV)
Te⊥ Te||
(g)
ions (eV)
(h)
180° elec (eV)
(i)
90° elec (eV)
(j)
0° elec (eV)
(k)
energy flux (s^3 cm^-2 ster^-1)
E_LMN (mV/m)
E_L E_M E_N
(l)
hhmm
2010 Oct 31
1649
1650
1651

Figure 4.

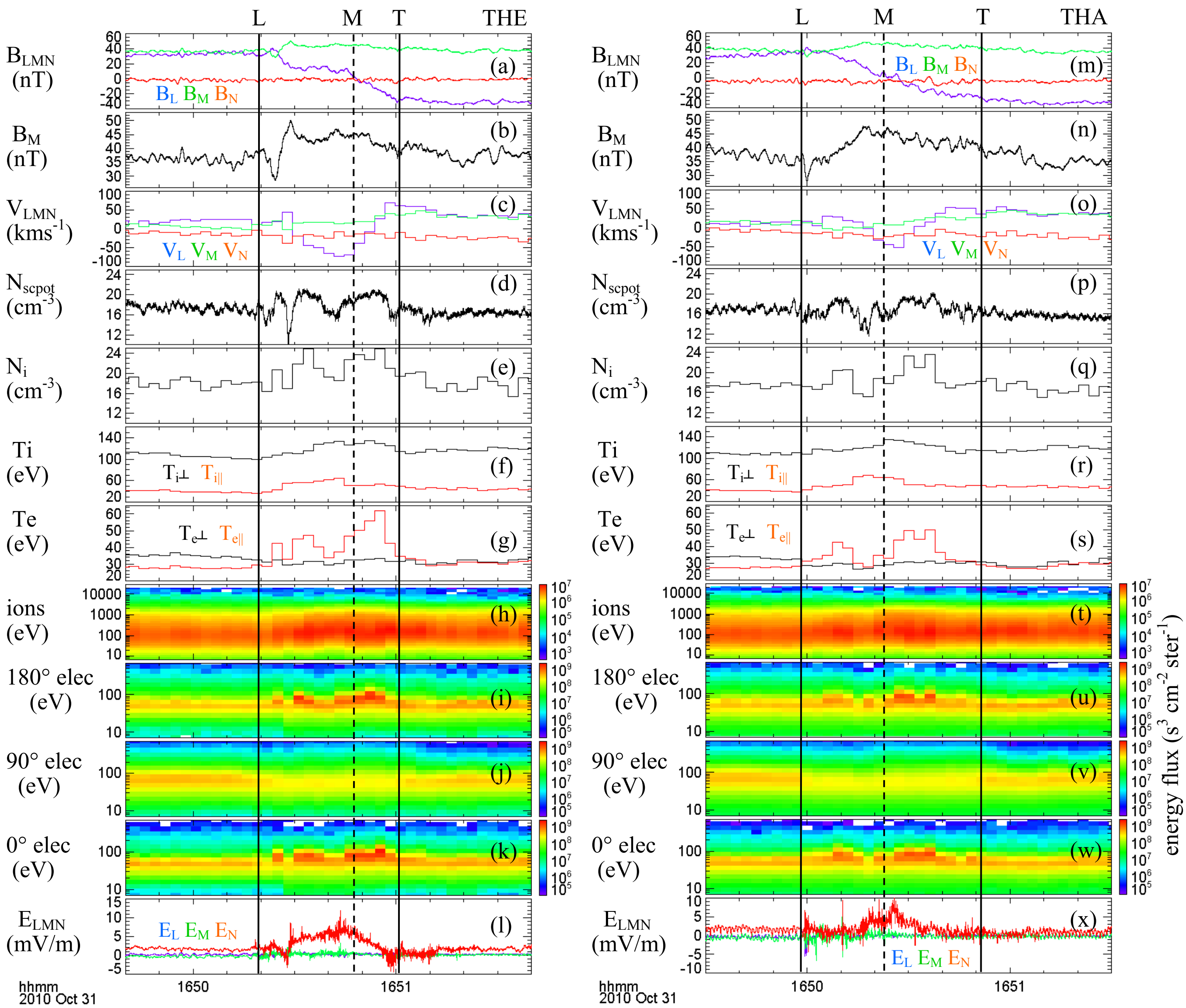

L M T THE
L M T THA
B_LMN (nT)
B_L B_M B_N
B_M (nT)
V_LMN (kms-1)
V_L V_M V_N
N_scpot (cm-3)
N_i (cm-3)
Ti (eV)
Ti⊥ Ti||
Te (eV)
Te⊥ Te||
ions (eV)
180° elec (eV)
90° elec (eV)
0° elec (eV)
E_LMN (mV/m)
E_L E_M E_N
energy flux (s3 cm-2 ster-1)
hhmm
2010 Oct 31
1650
1651